RAA 2019 Vol. **19** No. **12**, 184(9pp) doi: 10.1088/1674–4527/19/12/184

http://www.raa-journal.org *http://iopscience.iop.org/raa*

Research in Astronomy and Astrophysics

Estimation of the elastic thickness over ancient Mare Moscoviense

Zhen Zhong[1,2], Jian-Guo Yan[2,3⋆], Teng Zhang[1], Zhi-Yong Xiao[4], and Jose Alexis Palmero Rodriguez[5]

[1] School of Physics and Electronic Science, Guizhou Normal University, Guiyang 550001, China
[2] State Key Laboratory of Information Engineering in Surveying, Mapping and Remote Sensing,Wuhan University, Wuhan 430079, China; *jgyan_511@163.com, jgyan@whu.edu.cn*
[3] Instituto de Astronomiay Ciencias Planetarias de Atacama, Universidad de Atacama, Copayapu 485, Chile
[4] Planetary Science Institute, Chinese University of Geosciences (Wuhan), Wuhan 430074, China
[5] Planetary Science Institute, 1700 East Fort Lowell Road, Suite 106, Tucson, AZ 85719-2395, USA

Received 2019 April 2; accepted 2019 July 17

Abstract The Moscoviense basin is an atypical lunar impact basin with concentric rings of positive and negative gravity anomalies. This basin can provide insights into the inhomogeneous thermal activities across the farside of the Moon. Based on an updated spherical harmonic thin elastic-shell loading model, we used localized admittance analyses to estimate the elastic thickness as well as other associated selenophysical parameters for the Moscoviense basin. The high precision gravity and topography data employed in our estimation were collected by the Gravity Recovery and Interior Laboratory and the Lunar Orbiter Laser Altimeter missions. Our results indicate that the crust-mantle interface is mainly compensated by the prefilling depth rather than the observed surface topography. The results constrained within two standard deviations yielded a small load ratio ($\sim$0.168), a best-fit crustal thickness of 36.2 km, and an optimized crustal density of 3159.5 $\mathrm{kg\ m^{-3}}$. Such large density approaches the density of olivine-rich mantle materials, implying that the excavation of the Mare Moscoviense occurred during a basin-forming impact. The inversed elastic thickness at Mare Moscoviense was around 18 km, lower than the previous results ($\sim$60 km) found over Mare basins on the lunar nearside. These results indicate that extreme thermal activity existed during the Moscoviense basin-forming period such as reheating mechanisms from a double-impact process and mare volcanism.

Key words: Mare Moscoviense — localized admittance — thin elastic spherical shell — elastic thickness

1 INTRODUCTION

The Moscoviense Basin is an about 420–640 km diameter impact basin that is located in the lunar highland (central coordinates of 26°N, 147.6°E). It was formed about 4.1 billion years ago (Morota et al. 2009), and is located within the Feldspathic Highland Terrain (FHT) on the farside of the Moon (Konopliv et al. 2001). This basin is considered a mascon, as indicated by the Maria that occupies the basin's floor (Fig. 1(a)), where a corresponding positive gravity anomaly was first revealed by the Clementine mission (Zuber et al. 1994). Then the satellite-to-satellite Doppler tracking subsystem (RSAT) applied by the JAXA SELENE mission (Japan Aerospace Exploration Agency Selenological and Engineering Explorer) further revealed the central positive anomaly surrounded with a negative anomaly (Fig. 1(b)). Such annular positive and negative anomaly is inconsistent with the basins central low-lying floor ($\sim$3 km) (Fig. 1(a)). The anomaly is quite different with those in the nearside mare basins (Namiki et al. 2009). These anomalies were further confirmed in the unprecedentedly high resolution gravity field models from the Gravity Recovery and Interior Laboratory (GRAIL) mission (Zuber et al. 2013; Neumann et al. 2015). The significant difference of gravity anomaly between Moscoviense and other nearside mare basins attracts hundreds of researches, owing to its likely implication to the dichotomy in the thermal activity in the two sides (Namiki et al. 2009; Wieczorek et al. 2013). The Moscoviense Basin was selected as one of the sites for future landings and exploration (Calzada-Diaz & Mest 2013).

In the absence of in-situ measurements (Langseth et al. 1976), the heat flow on the lunar surface is estimated from

⋆ Corresponding author

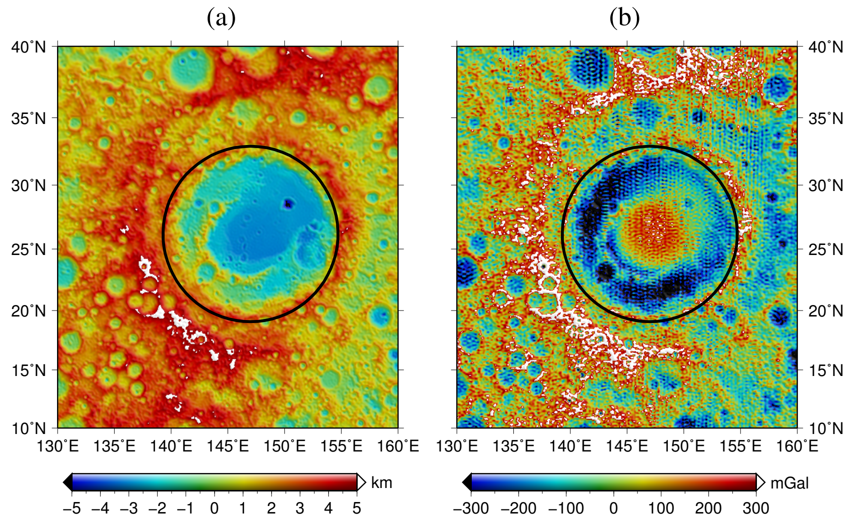

Fig. 1 Mercator projection of topography (a) from LOLA and free air gravity anomaly (b) from GL1500E. Mare Moscoviense is circled with an angular radius of 7°.

the effective elastic thickness (T_e) because it provides information on the time-scale during which the lithosphere relaxes, reaching the isostatic equilibrium (Watts 1994; McGovern et al. 2002). The elastic thickness is generally investigated through the admittance, which is estimated from topography and gravity data. (Belleguic et al. 2005; Grott & Wieczorek 2012; Huang & Wieczorek 2012; Zhong et al. 2014, 2018, 2019). This approach supposes that the lithosphere of the Moon behaves elastically as a spherical shell or an elastic plate. In terms of the inconsiderable support of lithospheric membrane stresses to loads, the lunar lithosphere is best modeled as a thin elastic spherical shell (Turcotte et al. 1981; Crosby & McKenzie 2005). The shell will deflect elastically according to surface and/or subsurface loads acting on it, and then producing a resultant gravity anomaly to calculate a modeled admittance function. By minimizing the misfit between the modeled admittance and observations, several parameters designating the properties of the lithosphere can be estimated. These include the crustal thickness (b_c) and density (ρ_c), load ratio (f) and the effective elastic thickness (T_e) (McGovern et al. 2002; Zhong et al. 2018, 2019).

Much research has focused on the constraints of these parameters. Crosby & McKenzie (2005) firstly measured elastic thickness nearside of the Moon overall, using a low-precision gravity of Lunar Prospector mission and topography from Clementine. With the improvements in gravity information accuracy from SELENE mission, Huang & Wieczorek (2012) evaluate the possible elastic thickness not only on the nearside but also on the farside of the Moon. Subsequently, a multi-parameter inversion based on Particle Swarm Optimization (PSO) algorithm was introduced by Zhong et al. (2014, 2019) to increase computational efficiency. These inversions are successful on highland areas with strong correlation between gravity and topography, but not mare basins or craters. The localized admittance and correlation spectrum over lunar basins or craters, especially mare basins, generally fluctuates between negative and positive values (Zhong et al. 2018). In such a case, the modeled admittance is not easily fitted with observations.

To deal with this problem, Zhong et al. (2018) referred the previous study of Huang & Wieczorek (2012), and introduced a subsurface load arising at the crust-mantle interface. In their study, the subsurface load was actually regarded as super-isostatic uplift. Their algorithm even employed the PSO to make multi-parameter inversion and successfully estimated the optimized parameters over Grimaldi basin. However, the challenge to the method still exists and makes it difficult to be widely applied due to complexity of selenophysical process. This is one of the reasons ascribed to the difficult estimation of prefilling basins' depth, which was used to describe the depth prior to mare filling. Zhong et al. (2018) took a relationship of depth/diameter to correct the gravity anomaly from ejected deposits. This method first tries to generate an ellipsoid according to the relation between the basins diameter and its possible depth. Taking the difference between the localized crustal density and its mean value of 2550 $\mathrm{kg\ m^{-3}}$, the gravity anomaly from ejected deposits can be measured and corrected from the surface free air gravity anomaly. However, this approach is insufficient when correcting gravity anomalies produced by ejected deposits in the Moscoviense Basin.

To estimate the deposits, we first take the bulk density of the highlands crust ($\sim$2550 $\mathrm{kg\ m^{-3}}$, Wieczorek et al. 2013) to remove gravitational contribution from surface topography. The updated topography data from Lunar

Orbiter Laser Altimeter (LOLA) instrument shows an unprecedented resolution with spherical harmonic expansion to degree 2050 (Smith et al. 2010), which is sufficient to correct surficial gravity anomaly. Then, the resulted gravity anomaly is Bouguer anomaly, which is mainly produced at the relief along the crust-mantle interface and density anomaly in the mantle. They can also be filtered by inversely using a minimum amplitude filter of Wieczorek & Phillips (1998), which is equivalent of a high-pass filter. Then, the rest of the anomaly is mainly formed of ejected deposits (Andrews-Hanna et al. 2013; Besserer et al. 2014), and can be used to invert the prefilling depth. This depth can be incorporated into the surface loading model, based on an updated version of the spherical harmonic thin elastic-shell. Combined with a subsurface loading model of super-isostatic uplift at crust-mantle interface, we can calculate modeled admittance and employ it to estimate the elastic thickness, as well as other associated parameters. This process is introduced in Section 2 and Appendix A. The inversion, parameters, results, and discussion are presented in Section 3. Finally, Section 4 summarizes our work and draws conclusions.

2 DATA AND METHODS

2.1 Data

The lunar gravity field models from the GRAIL mission were used in this study. The Jet Propulsion Laboratory (JPL) team recently provided the GL1500E model that is expanded to degree and order of 1500 (Park et al. 2015). The GL1500E gravity model has to a half-wavelength resolution of $\sim$ 3.6 km at the lunar surface. This was combined with the lunar topography data to estimate elastic thickness. The topography data was obtained from the LOLA instrument. The best resolution LOLA data has a spherical harmonic degree and order of 2050, which corresponds to a spatial resolution of 3 km. The GRAIL and LOLA data are available on the Geosciences Node of the NASA Planetary Data System (PDS).

2.2 Localized Admittance

Supposing h represents topography and g denotes the surface gravity, they can be expanded in the form of spherical harmonics. Supposing their spherical harmonic expansion coefficients are $g_{lm}$and h_{lm}, respectively, it can be written as

$$g(\Omega)=\sum_{ilm} g_{lm}Y_{lm}(\Omega), h(\Omega)=\sum_{ilm} h_{lm}Y_{lm}(\Omega)\,, \quad (1)$$

in which Y_{lm} represents the normalized spherical harmonics of degree l and order m, Ω denotes space angle of longitude ϕ and colatitudeθ, and i varies between 1 and 2 for the $\cos(m\phi)$ and $\sin(m\phi)$. According to the research of Wieczorek & Simons (2005); Wieczorek & Simons (2007) it is firstly needed to localize the global expanded gravity and topography in order to estimate parameters in a localized region. As to such region with an angular radius θ_0, the globally distrusted gravity and topography can be localized with an axisymmetric windowing function $\psi(\theta_0)$. It can be expanded with a normalized Legendre's polynomia $\psi_j\overline{p}_{j0}(\cos\theta_0)$ up to a maximum degree $l_{\rm win}$ (Wieczorek & Simons 2005; Wieczorek & Simons 2007).

$$\psi(\theta_0)=\sum_{j=0}^{l_{\rm win}}\psi_j\overline{p}_{j0}(\cos\theta_0)\,. \quad (2)$$

By multiplying the global data with a windowing function, we can get the localized gravity $g(\Omega)\psi(\theta_0)$ and localized topography $h(\Omega)\psi(\theta_0)$. Then we can estimate the cross-power $S_{\Phi\Gamma}(l)$ between the localized gravity and topography, which is given as (Wieczorek & Simons 2005; Wieczorek & Simons 2007)

$$\sum_{l=0}^{\infty}S_{\Phi\Gamma}(l)=\frac{1}{4\pi}\int_{\Omega}[\psi(\theta_0)g(\theta_0)][\psi(\theta_0)h(\theta_0)]\,{\rm d}\Omega\,. \quad (3)$$

Analogously, we can obtain the auto-power spectrum $S_{\Phi\Phi}(l)$ and $S_{\Gamma\Gamma}(l)$ for $g(\Omega)\psi(\theta_0)$ $h(\Omega)\psi(\theta_0)$, respectively. It is then likely to estimate the localized admittance $z(l)$ and correlation $\gamma(l)$ (Wieczorek & Simons 2005; Wieczorek & Simons 2007), which have the expression of

$$z(l)=\frac{S_{\Phi\Gamma}(l)}{S_{\Gamma\Gamma}(l)},\gamma(l)=\frac{S_{\Phi\Gamma}(l)}{\sqrt{S_{\Gamma\Gamma}(l)\cdot S_{\Phi\Phi}(l)}}\,. \quad (4)$$

According to the researches of Bendat & Piersol (1971), the error of localized admittance is rewritten as

$$\sigma_z^2(l)=\frac{S_{\Gamma\Gamma}(l)}{s_{\Phi\Phi}(l)}\frac{1-\gamma^2(l)}{2l}\,. \quad (5)$$

2.3 Misfit Function

We here modeled the lunar lithosphere as an elastic and thin spherical shell. Given a serial of estimated parameters mentioned above, we can evaluate a corresponding modeled gravity anomaly for the shell, which is described in Appendix A. In light of equations (2)–(5) and equations (7)–(9) in the recent study of Zhong et al. (2019), we can get the resulted gravity anomaly and its modeled admittance. By minimizing misfit between the modeled admittance and the observations, we can estimate the aforesaid parameters. According to the research of Belleguic et al. (2005), we take chi-squared as the misfit function, which is expressed as

$$\sigma^2=\frac{1}{N}\sum_{l=l_{\rm win}}^{l_{\rm max}}[\frac{z^{\rm obs}(l)-z^{\rm mod}(l)}{\sigma_z(l)}]^2\,, \quad (6)$$

in which the observed and modeled admittances are represented by $z^{\mathrm{obs}}(l)$ and $z^{\mathrm{mod}}(l)$, respectively, which have a degree l, and $\sigma_z(l)$ designates the observed admittance error of Equation (5). l_{max} is the maximum degree of the expanded gravity in Equation (1). Considering the four estimated parameters aforesaid, we have the relation $N = l_{\mathrm{max}} - 2l_{\mathrm{win}} - 4$ for the number of degrees of freedom. Due to the chi-squared function having a standard deviation near to $\sqrt{\frac{2}{N}}$, we can estimate the free parameters within $2\sigma_{\mathrm{STD}} = 2\sqrt{\frac{2}{N}}$.

2.4 Prefilling Depth Inversion

The observed surface free-air gravity anomaly over Moscoviense is mainly contributed by surface topography, ejected deposits and/or intrusion, topography at the Moho, and the mantle density anomaly (Thorey et al. 2015). The updated GRAIL gravity field model is expanded up to degree 1500 (Park et al. 2015), and its root-mean-square (RMS) spectrum is designated as GL1500e in Figure 2(a). Considering a finite-amplitude relief correction (Wieczorek & Phillips 1998) of the topography with a constant crustal density of 2550 $\mathrm{kg\ m^{-3}}$ (Wieczorek et al. 2013), we can estimate the gravitational contribution from the surface topography and subtract it from the free air gravity anomaly to obtain Bouguer anomaly. Then, we apply the low-pass filter of Wieczorek & Phillips (1998) to filter the Bouguer anomaly and the rest signals is mainly from deposits and/or intrusion. We parameterized the filter with a half value at a spherical harmonic degree λ, which is associated with the size of the studied basin. Different places generally show different values of λ. After many tests, we find that a best-fitting parameter can be found at the degree of 40 ($\lambda = 40$), with a corresponding spatial resolution (i.e., wavelength) of about 270 km.

More spherical harmonic coefficients of high degrees considered in calculation can amplify short wavelength noise in the gravitational field. Considering the Bouguer gravity of the updated GRAIL model is accurate to about degree 600 (Park et al. 2015), both the gravity field model and topography are truncated at the degree and order of 449. We also consider a cosine filter to remove short wavelength noise resulted from truncation between degree 400 and 449. The RMS spectrum of the filtered gravity model is represented by Filtered Bouguer in Figure 2(a). According to the study of Thorey et al. (2015), the Bouguer anomaly is actually a result of band-passed filtering. Its shortest and longest signals are mostly eliminated. Using Filtered Bouguer, we can inverse the prefilling depth of the basin using equation (18) of Wieczorek & Phillips (1998). The estimated subsurface topography under Moscoviense is shown in Figure 2(b), which shows the lowest depth at the basin's center.

3 RESULTS AND DISCUSSION

The research of Wieczorek et al. (2013) demonstrated that the lunar lithosphere deforms little for the loads beyond spherical harmonic degree and order 150. We thus truncated the gravitational and topographic models up to degree 150 (l_{max}=150). We took an angular radius of 7° to constrain the mare Moscoviense, which can contain all the gravitational features associated with its low-lying floor (Neumann et al. 2015). Such radius corresponds to a spherical harmonic bandwidth of 37. Considering removing long-wavelength variations in crustal density Wieczorek et al. (2013), the number of degrees of freedom analyzed here is close to 70, with a corresponding $2\sigma_{\mathrm{STD}}$ of 0.338. It means that the parameters can be best-estimated with an RMS misfit σ lower than 1.338. The ranges of these parameters and other nominal ones are listed in Table 1. In the localized admittance analysis, we merely considered a single localization window, which is employed in the previous study of Huang & Wieczorek (2012). To avoid leakage of power, we take a window whose power up to 99% concentrates within the targeted place.

To estimate best-fitted parameters, we first evaluate the subsurface topography at the crust-mantle interface to produce a synthetic gravity anomaly (Turcotte et al. 1981). The relief can be calculated according to observed surface topography or the possible prefilling depth (McGovern et al. 2002; Crosby & McKenzie 2005; Zhong et al. 2018, 2019). As the nonlinearity of the thin elastic spherical shell, Zhong et al. (2018) introduced an updated version of spherical harmonic thin elastic-shell loading model. Their model is not only useful in highland area, but is also applicable for Mare basins. Based on their research and after many tests, we find that it is possible to make a best-fitted estimation when considering crust-mantle relief compensated by the prefilling depth (h_0) of Figure 2(b) rather than observed surface topography ($\sim$depth after filling, h).

Based on previous research (Zhong et al. 2018), we consider four interfaces into our model to produce synthetic gravity anomaly. Reliefs of these interfaces are shown in Table 2 and their estimation can be processed according to Equations (A.1)–(A.15). Given a serial of parameters aforementioned, we can remove gravity anomaly from prefilling depth and produce a modeled admittance based on the left gravity anomaly in terms of Equations (A.1)–(A.3). To make a multi-parameter estimation, the modeled admittance was fitted with observation through a nonlinear algorithm Particle Swarm Optimization (PSO). After many tests, we take a trade-off swarm size of 400 and iterations of 50 to make a global op-

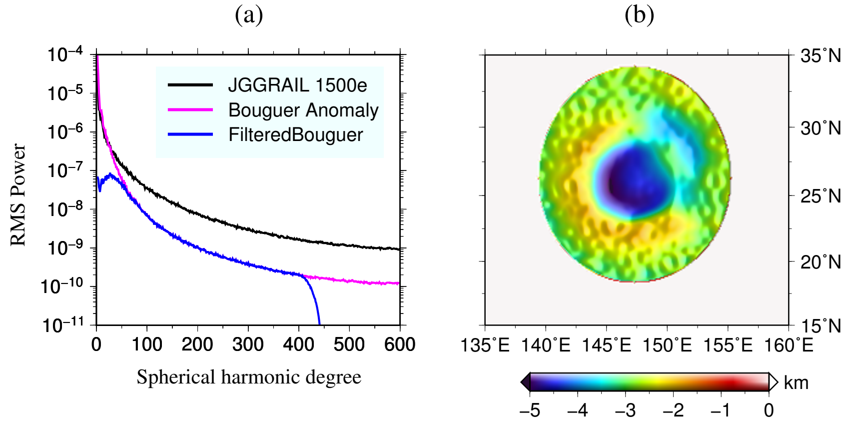

Fig. 2 Figure (a) represents power spectra for various gravity models. Black solid line: free-air gravity from the GRAIL gravity model JGGRAIL GL1500E. Magenta solid line: Bouguer gravity anomaly with a constant crustal density of 2550 $\mathrm{kg\ m^{-3}}$. Blue solid line: Filtered Bouguer anomaly with a low-passed filter parameter $\lambda = 40$ and a cosine filter to remove short wavelengths between 400 and 449. Figure (b) designates the inversed prefilling depth from Filtered Bouguer.

Table 1 Nominal Parameter Values

Parameter name	Value or range
Load ratio f	$-0.8\sim5$
Mean crustal density ρ_c ($\mathrm{kg\ m^{-3}}$)	2000∼3200
Mean crustal thickness b_c (km)	0.0∼60
Lithospheric elastic thickness T_e (km)	0.0∼150
Surface gravity acceleration g ($\mathrm{m\ s^{-2}}$)	1.721
Referenced radius R (km)	1737.15
Mass of the Moon M (kg)	$7.3458998185\times10^{22}$
Poisson's ratio of lithosphere υ	0.25
Young's modulus of lithosphere E (Pa)	1.0×10^{11} (McGovern et al. 2002)
Density of filling deposit ρ_s ($\mathrm{kg\ m^{-3}}$)	3200 (Namiki et al. 2009)
Mantle density ρ_m ($\mathrm{kg\ m^{-3}}$)	3220 (Wieczorek et al. 2013)

Table 2 The Referenced Interfaces Utilized in the Calculation of Modeled Gravity Anomaly

No	Interface	Relief of interface	Density contrast	Referenced radius
1	Prefilling depth	h_0	ρ_c	R
2	Crust-Mantle interface	$-(h_\mathrm{b}+w_\mathrm{t})$	$\rho_\mathrm{m}-\rho_\mathrm{c}$	$R-b_\mathrm{c}$
3	Subsurface load	w_b	ρ_b	$R-z_\mathrm{b}$
4	Referenced layer of subsurface load	$-(h_\mathrm{b}+w_\mathrm{t})$	$-\rho_\mathrm{b}$	$R-z_\mathrm{b}$

timization. The result indicates that the best-fitted crustal thickness is around 36.2 km, with a corresponding best value of density about 3159.5 $\mathrm{kg\ m^{-3}}$. The best-evaluated load ratio is found quite small, close to 0.168. The best-inversed T_e is about 18 km, smaller than those thicknesses over the mare basins on the nearside of the Moon (Sugano & Heki 2004).

The best-fitted crustal thickness and density are about 36.2 km and 3159.5 $\mathrm{kg\ m^{-3}}$, respectively. A small surface to subsurface load ratio of 0.168 is found and the elastic thickness is constrained around 18 km.

The best-fitted spectrum between the modeled admittance and observation is shown in Figure 3. The spectra of admittance and correlation present an intuitive fluctuation between negative and positive values.The observed admittance spectrum shows a decline steeply from the beginning to the degree 51, where the admittance value even gets close to –450 mGal $\mathrm{km^{-1}}$. It climbs until degree 58 where the admittance is near to the maximum value ($\sim$150 mGal $\mathrm{km^{-1}}$) but shows another descent towards larger degrees. Then, it ascends at the degree 70 where the admittance value approaches to -18 mGal $\mathrm{km^{-1}}$ and stops to decline sharply until degree 102. Over the rest degrees, it even rises steadily again. It is evident that the best-fitted admittance spectrum behaves similarly with the observation. The corresponding misfit σ is close to 1.296 which is lower than $2\sigma_\mathrm{STD}$ of 1.338. Therefore, the elastic thickness (T_e) associated with other parameters including crustal thickness (b_c) and density (ρ_c), and load ratio (f) is well constrained within $2\sigma_\mathrm{STD}$.

For the purpose of testing acceptable ranges, Figure 4 carried out a trade-off study. Figure 4(a) gives a trade-off

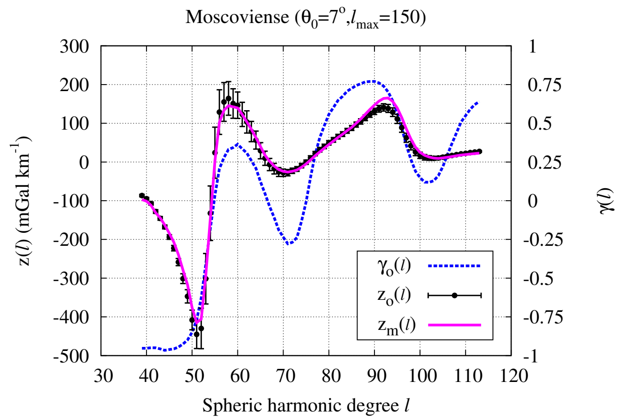

Fig. 3 Correlation spectrum observed (*dashed line*), admittance spectrum observed (*error bar*) and admittance spectrum modeled (*solid line*) for Mare Moscoviense with a maximum degree of 150.

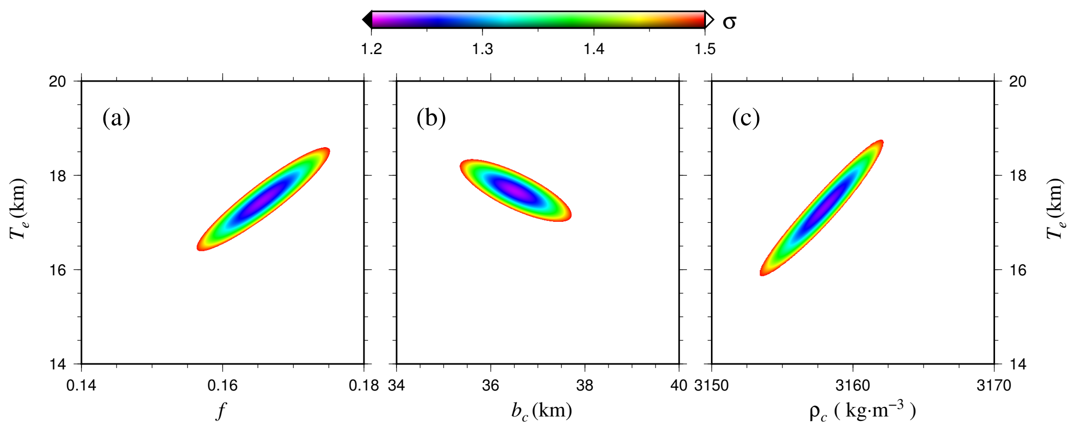

Fig. 4 RMS misfits σ in the trade-off studies between (a) $T_{\rm e}$ vs. f, (b) $T_{\rm e}$ vs. $b_{\rm c}$, and (c) $T_{\rm e}$ vs. $\rho_{\rm c}$.

variation between $T_{\rm e}$ and f. It can be found that the best-fitted elastic thickness $T_{\rm e}$ ranges from 16.8 km to 18 km, while f varies between 0.16 and 0.172. The elastic thickness in Figure 4(b) varies between 17.5 km and 18 km, where the crustal thickness changes from 35.8 km to 37.2 km. In the rest panel of Figure 4, the elastic thickness fluctuates in a relatively wide range from 16.4 km to 18.1 km, and the well constrained crustal density falls in the range from 3155 $\rm kg\ m^{-3}$ to 3160 $\rm kg\ m^{-3}$.To further study the ranges of parameters, Figure 5(a) and Figure 5(b) demonstrate a load ratio (f) of $0.618^{+0.0023}_{-0.0018}$ and a crustal thickness ($b_{\rm c}$) of $36.2^{+0.3}_{-0.3}$ km, respectively. Such low value of load ratio found here is a result of high density of crust. As aforementioned, the subsurface is regarded as super-isostatic uplift at the crust-mantle interface. It is noted that the crustal density is around 3159 from Figure 4(c) and Figure 5(c), closing to the value of lunar mantle. It is therefore difficult to distinguish the crust-mantle interface and accordingly impossible to recognize the subsurface load. As the crustal thickness found here, it is actually equivalent to a regional mean value (Turcotte et al. 1981). Our result is quite close to the mean crustal thickness (∼40 km) around Moscoviense in the research of Wieczorek et al. (2013) and Miljković et al. (2015).

Figure 5(c) exhibits a best-fitted crustal density ranging from 3158.7 $\rm kg\ m^{-3}$ to 3160 $\rm kg\ m^{-3}$. This result also approaches to the studies of Wieczorek et al. (2013) and Miljković et al. (2015). Analyses of lunar mare basalts (Longhi 1992), as well as simulations of magma ocean crystallization (Elkins-Tanton et al. 2011) imply olivine as one of the minerals composing the lunar upper mantle. This conclusion has been supported by the inversions of seismic travel-time data (Khan et al. 2007; Kronrod & Kuskov 2011). It is also approved by the observations from Kaguya mission (Yamamoto et al. 2010, 2012) and from Chandrayaan-1 spacecraft (Bhatt et al. 2018). Recent numerical simulations have confirmed the excavation of lunar upper mantle over Moscoviense as well (Miljković et al. 2015). The best-fitted crustal density found here (∼3159.5 $\rm kg\ m^{-3}$) is close to the density of olivine, indicating the possible excavation of mare Moscoviense during its basin-forming impact.

The rest panel of Figure 5(d) displays an elastic thickness varying between 17.7 km and 18.1 km. This value is

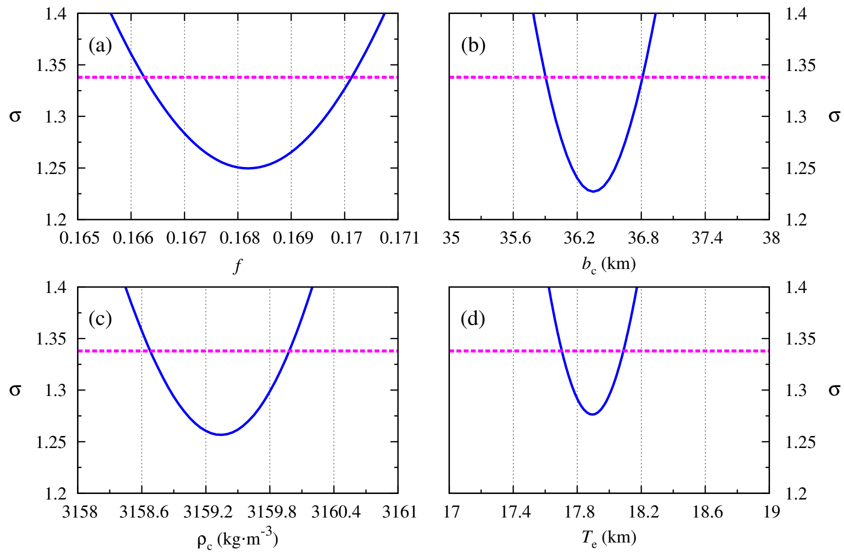

Fig. 5 Minimized misfits σ for the analyzed Mare Moscoviense. Panels (a-d) are σ distributions concerning load ratio f, crustal thickness b_c, crustal density ρ_c, and elastic thickness T_e. Here the dashed lines represent $2\sigma_{STD}$.

quite lower than previous results ($\sim$60 km) over mare locations on the nearside of the Moon (Arkani-Hamed 1998; Sugano & Heki 2004). Such abnormal small elastic thickness means distinct selenophysical process between mare Moscoviense and other mare basins on the nearside. Using the first high-precision gravity from SELENE mission, Ishihara et al. (2011) proposed an alternative hypothesis of double impact scenario for the Moscoviense basin formation. This hypothesis not only accounts for the anomalously large mantle plug beneath the basin but it also answers the asymmetric surface geomorphology and excavation of olivine rich material. Contemporaneously, not only Ishihara et al. (2011) but also Thaisen et al. (2011) supported the possible formation of multiple impacts. If Moscoviense did experience such scenario of double or multiple impacts, the later impact would reheat the basin and weaken the flexural rigidity built at the first impact. Additionally, the mare volcanism could ascribe to the small elastic thickness. The researches of Morota et al. (2009) and Taguchi et al. (2017) indicated that most of the mare basalts erupted for 200 Ma after the mare basins formation. The long-term volcanism could greatly heat the base of the mare basins, even leading to magma intrusion into the crust. The high crustal density of 3159.5 $\mathrm{kg\ m^{-3}}$ estimated here could possibly be the result of this process. Considering the extraordinary heating process of multiple impacts and mare volcanism, the ancient lithosphere over mare Moscoviense could develop quite thin and the small elastic thickness estimated here would be reasonable.

4 CONCLUSIONS

In this study, we utilize a localized admittance analysis to inverse elastic thickness as well as associated parameters over Mare Moscoviense. Based on an updated version of spherical harmonic thin elastic-shell loading models, we have successfully fitted the modeled admittance with observation. This result indicates that the crust-mantle interface is mainly compensated by the prefilling depth (h_0) rather than the observed surface topography h. Constrained within $2\sigma_{STD}$, a small load ratio (~ 0.168) is found here. The mean value of best-fitted crustal thickness gets close to 36.2 km, which is near to other results (~ 40 km) from GRAIL. The global optimal solution of crustal density is around 3159.5 $\mathrm{kg\ m^{-3}}$, coinciding with other results from GRAIL. Such relatively large density approaches to the density of olivine which is observed as one of the minerals from the lunar upper mantle. This result implies the possible excavation of Mare Moscoviense during its basin-forming impact. A best-inversed elastic thickness is discovered to be surrounding 18 km. This small value is quite lower than previous results (~ 60 km) over the nearside mare basins. It indicates an extreme thermal activity existed during the Moscoviense basin-forming period, for example, the reheating mechanism during the possible double-impact process and mare volcanism. This result can be of great significances to understand the inhomogeneous thermal evolution on the Moon.

Acknowledgements The authors would like to thank the scientific teams from LRO and GRAIL missions who have provided the topography and gravity data employed in this research. These data are downloaded from PDS website. All the figures in this study are produced with the Generic Mapping Tools (GMT) package. The freely available software archive SHTOOLS was employed to take the localized analysis. This research are supported by the National Natural Science Foundation of China (41864001 and U1831132), Guizhou Science and Technology Plan Project (Guizhou Science and Technology platform talents [2018]5769), Open Fund of State Laboratory of Information Engineering in Surveying, Mapping and Remote Sensing, Wuhan University (Grant No. 17P03), Open Fund of Key Laboratory of Environment Change and Resources Use in Beibu Gulf, Ministry of Education (Guangxi Teachers Education University) and Guangxi Key Laboratory of Earth Surface Processes and Intelligent Simulation (Guangxi Teachers Education University, No. 2015K03), Open Fund of Guizhou Provincial Key Laboratory of Radio Astronomy and Data Processing (KF201813), Open Fund of Lunar and Planetary Science Laboratory, Macau University of Science and Technology (FDCT 119/2017/A3), and Hubei Province Foundation innovation group project (2018CFA087).

Appendix A: APPENDIX A. GOVERNING EQUATION AND MODELED GRAVITY

Due to the support of membrane stresses to loads, Turcotte et al. (1981) and Zhong & Zuber (2000) demonstrated that the lunar lithosphere is better modeled as a thin and elastic spherical shell. Supposing the lunar lithosphere corresponds to a load q (positive downward) with a defection $w_{\rm L}$ (positive downward), Kraus & Kalnins (1968) and Turcotte et al. (1981) derived the governing equation of the shell, which is expressed as

$$\begin{aligned} &D\nabla^6 w_{\rm L} + 4D\nabla^4 w_{\rm L} + ET_{\rm e}R^2\nabla^2 w_{\rm L} + 2ET_{\rm e}R^2 w_{\rm L} \\ &= R^4[(\nabla^2+2)-(1+\nu)]q \end{aligned} \tag{A.1}$$

in which the reference radius of the shell is designated by R, Yong's modulus is denoted by E, Poisson's ratio is represented by ν, and the flexural rigidity is designated by D which has the relation $D = \frac{ET_{\rm e}^3}{12(1-\nu)^2}$.

Not only does surface load cause the deflection of the lithosphere, but also subsurface load (Forsyth 1985). We here suppose $h_{\rm i}$ represents the initial topography of the surface load and $w_{\rm i}$ denotes the initial relief of the subsurface load. Also imaging $h_{\rm t}$ and $w_{\rm b}$ are their heights after loading, their corresponding lithospheric deflection $w_{\rm t}$ and $h_{\rm b}$ can be deduced as (Forsyth 1985)

$$h_{\rm i} = h_{\rm t} + w_{\rm t} \tag{A.2}$$

$$w_{\rm i} = w_{\rm b} + h_{\rm b} \tag{A.3}$$

We here assume that the lunar crust-mantle interface is compensated before ejected deposits infilling the basins. Then, we can obtain the prefilling depth h_0 and subsurface load interface w as follows:

$$h_0 = h_{\rm t} - h_{\rm b} \tag{A.4}$$

$$w = w_{\rm b} - w_{\rm t} \tag{A.5}$$

The actual lithosphere deflection is likely produced by the combination of the surface and subsurface loads. We here introduced a model involving four interfaces, which is shown in Table 2. The quantities of $b_{\rm c}$ and $z_{\rm b}$ represent the crustal thickness and subsurface load depth, respectively. Imagining subsurface load generates at the crust-mantle interface, we can have the relationship $b_{\rm c} = z_{\rm b}$. Accordingly, the total pressure generated is

$$q = g[\rho_{\rm c}h_0 - (\rho_{\rm m}-\rho_{\rm c})(h_{\rm b}+w_{\rm t}) + \rho_{\rm b}(w_{\rm b}-w_{\rm t}) + \rho_{\rm b}(h_{\rm b}+w_{\rm t})] \tag{A.6}$$

in which $\rho_{\rm b}$ is the density contrast between the subsurface load and its surroundings. According to prefilling depth h_0, we can solve Equation (A.1) by the introduction of load-ratio f, which is defined as (Forsyth 1985)

$$f = \frac{\rho_{\rm b} w_{\rm i}}{\rho_{\rm c} h_{\rm i}} \tag{A.7}$$

Taking Equations (A.1)–(A.7) into account, the lithosphere will deflection with a value of $w_{\rm L}$. It can be written as (Zhong et al. 2018)

$$w_{\rm L} = -k_1 \cdot h_0 - k_2 \cdot w \tag{A.8}$$

where

$$k_1 = \frac{f\rho_{\rm c}}{f\rho_{\rm c} + \rho_{\rm m} - \rho_{\rm c}} \tag{A.9}$$

$$k_2 = \frac{\rho_{\rm m} - \rho_{\rm c}}{f\rho_{\rm c} + \rho_{\rm m} - \rho_{\rm c}} \tag{A.10}$$

Equation (A.1) is a typical nonlinear equation and no exact solutions exist. However, it can be solved as spherical harmonic form when assuming the estimated parameters being isotropic (McGovern et al. 2002; Huang & Wieczorek 2012). Supposing the subsurface load interface w can be expanded in spherical harmonics and imagining w_{lm} is its expanding coefficient, then we can have the relation (Zhong et al. 2018)

$$W_{lm} = -\frac{k_3(l)}{k_4(l)} h_{0,lm} \tag{A.11}$$

where

$$k_3(l) = \sigma k_1 \cdot \lambda_1(l) + \tau k_1 \cdot \lambda_2(l) + \frac{\rho_c}{\rho_m - \rho_c}\lambda_3(l) \tag{A.12}$$

$$k_4(l) = \sigma k_2 \cdot \lambda_1(l) + \tau k_2 \cdot \lambda_2(l) + \lambda_3(l) \tag{A.13}$$

$$\sigma = \frac{D}{gR^4(\rho_{\rm m} - \rho_{\rm c})} \tag{A.14}$$

$$\tau = \frac{ET_{\rm e}R^2}{gR^4(\rho_{\rm m} - \rho_{\rm c})} \tag{A.15}$$

where $h_{0,lm}$ is the spherical harmonic coefficient with degree l and order m of the prefilling depth h_0. Other quantities of $\lambda_1(l)$, $\lambda_2(l)$ and $\lambda_3(l)$ are referred as those in the recent study of Zhong et al. (2018). Given a serial of estimated parameters such as f, b_c, ρ_c and T_e, it can be estimated the resulted amplitudes of interfaces in Table 2 as well as the corresponding surface gravity anomaly. These anomalies can be estimated according section 2.3 in the research of Zhong et al. (2019).

References

Andrews-Hanna, J. C., Asmar, S. W., Head, J. W., et al. 2013, Science, 339, 675

Arkani-Hamed, J. 1998, J. Geophys. Res., 103, 3709

Belleguic, V., Lognonné, P., & Wieczorek, M. 2005, Journal of Geophysical Research (Planets), 110, E11005

Bendat, J. S., & Piersol, A. G. 1971, Random Data: Analysis and Measurement Procedures. 2nd ed., exp. & rev (Wiley)

Besserer, J., Nimmo, F., Wieczorek, M. A., et al. 2014, Geophys. Res. Lett., 41, 5771

Bhatt, M., Wöhler, C., Dhingra, D., et al. 2018, Icarus, 303, 149

Calzada-Diaz, A., & Mest, S. C. 2013, in Lunar and Planetary Inst. Technical Report, 44, Lunar and Planetary Science Conference, 1275

Crosby, A., & McKenzie, D. 2005, Icarus, 173, 100

Elkins-Tanton, L. T., Burgess, S., & Yin, Q.-Z. 2011, Earth and Planetary Science Letters, 304, 326

Forsyth, D. W. 1985, J. Geophys. Res., 90, 12623

Grott, M., & Wieczorek, M. A. 2012, Icarus, 221, 43

Huang, Q., & Wieczorek, M. A. 2012, Journal of Geophysical Research (Planets), 117, E05003

Ishihara, Y., Morota, T., Nakamura, R., Goossens, S., & Sasaki, S. 2011, Geophys. Res. Lett., 38, L03201

Khan, A., Connolly, J. A. D., Maclennan, J., & Mosegaard, K. 2007, Geophysical Journal International, 168, 243

Konopliv, A. S., Asmar, S. W., Carranza, E., Sjogren, W. L., & Yuan, D. N. 2001, Icarus, 150, 1

Kraus, H., & Kalnins, A. 1968, Journal of Applied Mechanics, 35, 624

Kronrod, V. A., & Kuskov, O. L. 2011, Izvestiya Physics of the Solid Earth, 47, 711

Langseth, M. G., Keihm, S. J., & Peters, K. 1976, in Lunar and Planetary Science Conference Proceedings, 7, ed. D. C. Kinsler, 3143

Longhi, J. 1992, Geochim. Cosmochim. Acta, 56, 2235

McGovern, P. J., Solomon, S. C., Smith, D. E., et al. 2002, Journal of Geophysical Research (Planets), 107, 5136

Miljković, K., Wieczorek, M. A., Collins, G. S., et al. 2015, Earth and Planetary Science Letters, 409, 243

Morota, T., Haruyama, J., Honda, C., et al. 2009, Geophys. Res. Lett., 36, L21202

Namiki, N., Iwata, T., Matsumoto, K., et al. 2009, Science, 323, 900

Neumann, G. A., Zuber, M. T., Wieczorek, M. A., et al. 2015, Science Advances, 1, e1500852

Park, R. S., Konopliv, A. S., Yuan, D. N., et al. 2015, in AGU Fall Meeting Abstracts, Vol. 2015, G41B

Smith, D. E., Zuber, M. T., Neumann, G. A., et al. 2010, Geophys. Res. Lett., 37, L18204

Sugano, T., & Heki, K. 2004, Geophys. Res. Lett., 31, L24703

Taguchi, M., Morota, T., & Kato, S. 2017, Journal of Geophysical Research (Planets), 122, 1505

Thaisen, K. G., Head, J. W., Taylor, L. A., et al. 2011, Journal of Geophysical Research (Planets), 116, E00G07

Thorey, C., Michaut, C., & Wieczorek, M. 2015, Earth and Planetary Science Letters, 424, 269

Turcotte, D. L., Willemann, R. J., Haxby, W. F., et al. 1981, J. Geophys. Res., 86, B5

Watts, A. B. 1994, Geophysical Journal International, 119, 648

Wieczorek, M. A., & Phillips, R. J. 1998, J. Geophys. Res., 103, 1715

Wieczorek, M. A., & Simons, F. J. 2005, Geophysical Journal International, 162, 655

Wieczorek, M. A., & Simons, F. J. 2007, Journal of Fourier Analysis & Applications, 13, 665

Wieczorek, M. A., Neumann, G. A., Nimmo, F., et al. 2013, Science, 339, 671

Yamamoto, S., Nakamura, R., Matsunaga, T., et al. 2010, Nature Geoscience, 3, 533

Yamamoto, S., Nakamura, R., Matsunaga, T., et al. 2012, Geophys. Res. Lett., 39, L13201

Zhong, S., & Zuber, M. T. 2000, J. Geophys. Res., 105, 4153

Zhong, Z., Li, F., Yan, J., Yan, P., & Dohm, J. M. 2014, Advances in Space Research, 54, 770

Zhong, Z., Yan, J.-G., Alexis, J., & Rodriguez, P. 2019, RAA (Research in Astronomy and Astrophysics), 19, 009

Zhong, Z., Yan, J., Rodriguez, J. A. P., & Dohm, J. M. 2018, Icarus, 309, 411

Zuber, M. T., Smith, D. E., Lemoine, F. G., & Neumann, G. A. 1994, Science, 266, 1839

Zuber, M. T., Smith, D. E., Watkins, M. M., et al. 2013, Science, 339, 668